nature communications

Article

https://doi.org/10.1038/s41467-026-71321-2

Global hotspots of particulate organic carbon losses under climate change

Received: 18 June 2025

Accepted: 19 March 2026

Published online: 01 April 2026

Check for updates

A list of authors and their affiliations appears at the end of the paper

Soil organic carbon (SOC) comprises particulate (POC) and mineral-associated organic carbon (MAOC), which differ in formation, stabilization, and loss mechanisms. While the current global distribution of POC and MAOC is characterized, their vulnerability under future climate scenarios remains unclear. Using 3284 topsoil (0-30 cm) observations from six continents, we identify high-latitude soils as global hotspots of SOC vulnerability under shared socioeconomic pathway scenarios (SSP126, SSP245, and SSP585). Under a high-emission scenario (SSP585), high-latitude soils are projected to lose substantial POC by 2100, accounting for about 81 ± 10% of total SOC losses. These declines are driven by the high proportion of SOC stored as POC (f_{POC}) and its high temperature sensitivity. We show that f_{POC} is a robust indicator of SOC vulnerability to climate change. Globally, the projected POC decline corresponds to a cumulative carbon dioxide (CO_2) release of 81.34 Pg CO_2-equivalent by 2100, highlighting the importance of preserving POC to mitigate climate feedbacks.

Soil organic carbon (SOC) plays a critical role in the global carbon cycle and supports key ecosystem functions[1,2], including soil health, water retention, and nutrient cycling[3–5]. While extensive research has focused on predicting the SOC responses to climate change, significant uncertainty remains[6,7]. This uncertainty is partly due to the complexity of the physicochemical stabilization of SOC[8]. The diverse SOC fractions within the intricate soil matrix create challenges in identifying the environmental factors that regulate global SOC dynamics under climate change[9].

The conceptual partitioning of SOC into particulate organic carbon (POC) and mineral-associated organic carbon (MAOC) has greatly advanced understanding of SOC dynamics[10,11]. These two fractions differ in their formation mechanisms, chemical compositions, turnover rates, and ecological functions[12,13]. MAOC is protected by mineral associations[14–16], making it less available to soil microorganisms and therefore more persistent than POC[10,17,18]. In contrast, POC exists in a free state without mineral protection[8,13] or is embedded within aggregates[19–21].

Recent experimental evidence indicates that POC, particularly free POC, is considerably more sensitive to temperature changes than MAOC[22,23]. Because of its lower bioavailability and typically larger contribution to SOC, MAOC has received greater attention in global assessments of SOC distribution, key drivers, and climate responses, especially as a key target for SOC accrual[24–26]. However, POC can also constitute a large fraction of SOC, especially in high-latitude soils, where its loss could amplify carbon-climate feedbacks[27]. Understanding how POC responds to future climate change is therefore crucial for predicting SOC vulnerability and guiding strategies to preserve soil carbon stocks.

Climate factors, particularly mean annual temperature (MAT) and mean annual precipitation (MAP), are key determinants of both POC and MAOC distributions (Supplementary Table 1). Previous studies suggest that POC may constitute the dominant SOC fraction in high-latitude soils and in soils where microbial growth and activities are limited by low temperatures and lack of oxygen[10,28,29]. For instance, by analyzing 155 paired POC-MAOC observations, García-Palacios et al. found that POC predominates across cold regions[27]. Combining these observations with data from experimental warming studies, they further demonstrated that the substantial SOC losses observed under warming are largely attributable to the dominance and high climate sensitivity of POC in these environments[27]. These findings underscore the importance of jointly examining the global distributions, controlling factors, and climate responses of POC and MAOC. Such a multi-pool approach is essential to improve predictions of SOC dynamics

e-mail: chenji@ieecas.cn

and advance the understanding of soil carbon management strategies under a changing climate[30,31].

Here, we compiled a comprehensive global database of topsoil (0–30 cm) POC and MAOC stocks. The database includes 3284 observations, including 2724 data points obtained from published studies (1987–2024) and 560 unpublished data points contributed by individual researchers. It encompasses all major terrestrial biomes and spans a broad gradient of MAT and MAP (Fig. 1b), enabling robust assessment of how key environmental drivers influence POC and MAOC distributions and their projected changes under future climate scenarios. Using a machine learning approach, we evaluated the relative importance of soil, plant, climate, and land cover variables in shaping global patterns of POC, MAOC, and the fraction of POC relative to total SOC (f_{POC}; see "Methods"). We then extrapolated current global distributions based on these empirical relationships and projected changes in POC, MAOC, and f_{POC} under three Shared Socioeconomic Pathways (SSPs). Specifically, SSP126 represents a sustainable, low-emission future; SSP245 a moderate mitigation scenario; and SSP585 a high-emission trajectory with limited climate policy intervention (O'Neill et al., 2016). Our analyses identify regions most vulnerable to future POC- and MAOC-related carbon losses, offering insights into global soil carbon management and strategies for mitigating climate-carbon feedbacks.

Results

Predictors of POC and MAOC stocks

Given the large variation in POC and MAOC stocks across the globe (Fig. 1c, d), we used random forest (RF) models to quantify the importance of 16 predictors (Supplementary Table 2), including climate, soil, plant, and land cover variables, and their interactions, accounting for covariation across predictors and potential nonlinearities. We found that land cover and MAT are the most significant determinants of global POC and MAOC stocks (Fig. 2a, b). A RF model trained exclusively with high-latitude data indicates that MAT remains a key driver of POC stocks in high-latitude soils, highlighting its central role in controlling POC distribution across this region (Supplementary Fig. 1).

High-latitude soils (north of 60° N or south of 60° S) contained substantial stocks of POC ($5.55 \pm 0.73\ kg\ m^{-2}$) and MAOC ($5.89 \pm 0.55\ kg\ m^{-2}$), leading to an f_{POC} of $49 \pm 3\%$, which is higher than that observed in lower latitude soils (Supplementary Fig. 2). Among land cover types, tundra soils had the highest POC ($9.36 \pm 1.52\ kg\ m^{-2}$) and MAOC ($7.80 \pm 1.02\ kg\ m^{-2}$) stocks, resulting in a larger f_{POC} ($55 \pm 4\%$) compared to other land covers (Supplementary Fig. 3). Boreal forest soils stored much more POC ($6.66 \pm 0.48\ kg\ m^{-2}$) and exhibited higher f_{POC} ($60 \pm 1\%$) than temperate and tropical forest (Supplementary Fig. 4). Both POC and MAOC stocks declined with increasing MAT,

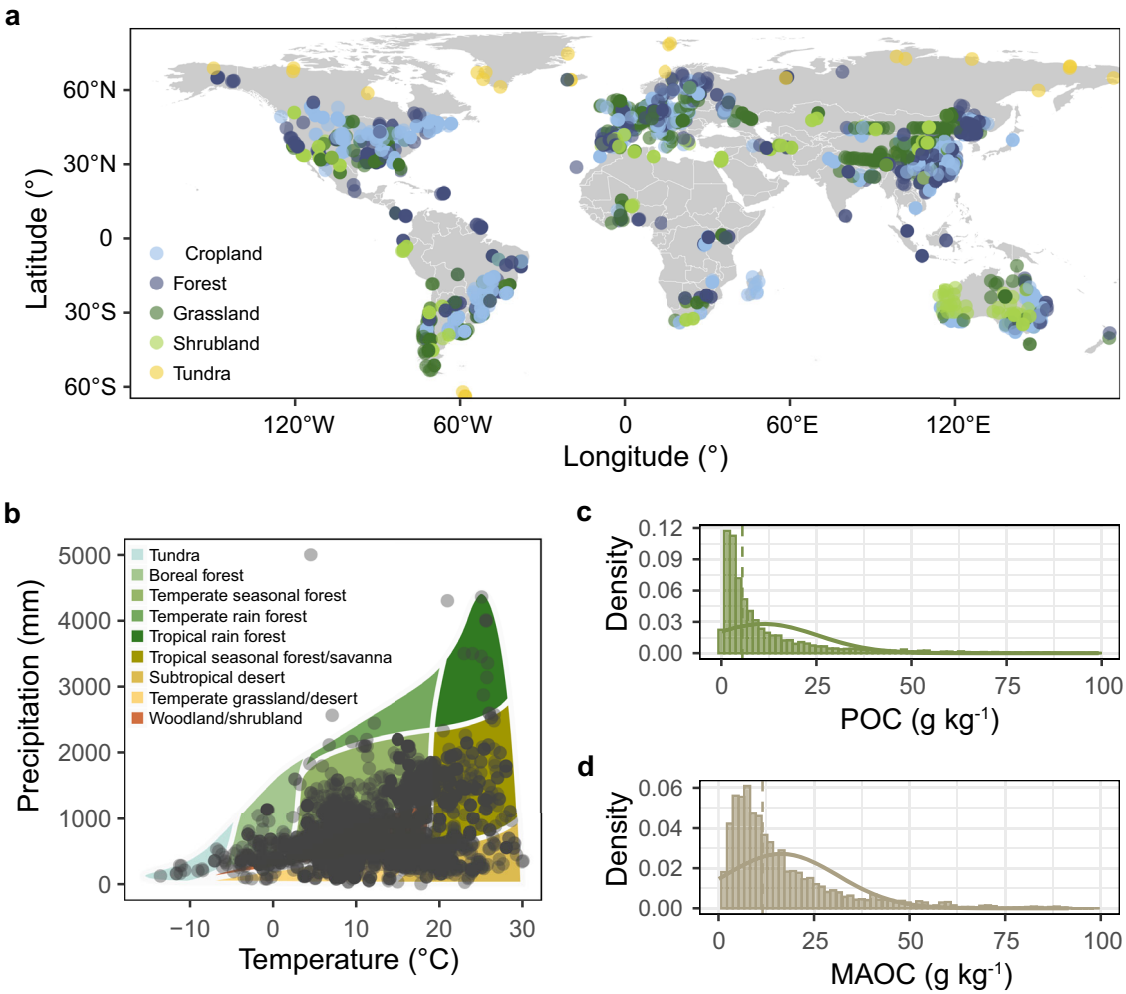

Fig. 1 | Geographic and climatic distribution of topsoil particulate organic carbon (POC) and mineral-associated organic carbon (MAOC) contents in the database. a Global distribution of 3284 observations. Different colors represent the land cover type assigned to each point based on author-reported plant community composition and management information. **b** Climate distribution of the soil sampling sites with a wide range of mean annual temperature and mean annual precipitation. **c**, **d** The dashed line in panels indicates the median of POC and MAOC content. The measurements were collected from literature studies and unpublished experimental data (Supplementary References).

https://doi.org/10.1038/s41467-026-71321-2

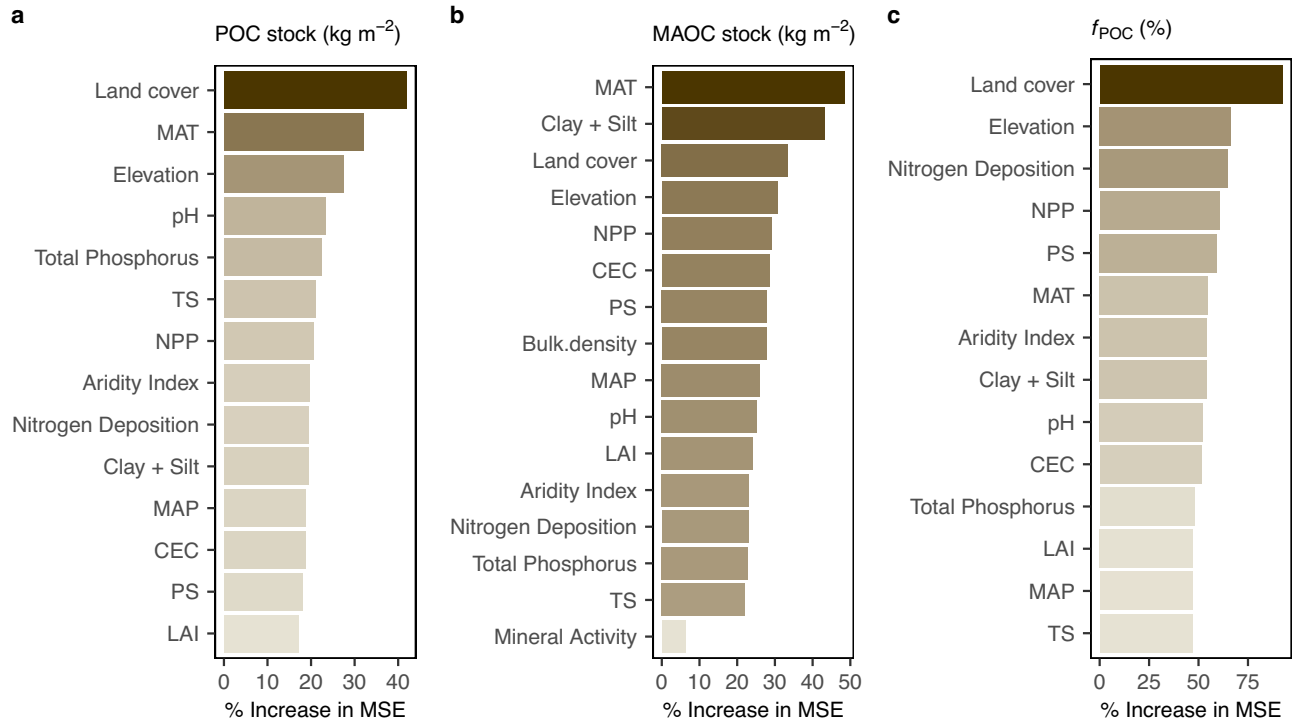

Fig. 2 | Variable importance of the random forest models for topsoil particulate organic carbon (POC) stock, mineral-associated organic carbon (MAOC) stock, and the proportion of POC relative to soil organic carbon (f_{POC}). a, **b**, **c** The importance of predictors for POC, MAOC, and f_{POC}. Mean annual temperature (MAT), mean annual precipitation (MAP), temperature seasonality (TS), precipitation seasonality (PS), elevation, background nitrogen deposition (nitrogen deposition), aridity index, cation exchange capacity (CEC), percent of clay and silt (clay + silt), total phosphorus, net primary productivity (NPP), soil pH, and leaf area index (LAI) are continuous variables. Land cover and mineral activity (high activity minerals and low activity minerals) are categorical variables. Variable importance is ranked by the percent increase in mean square error (MSE).

but POC stock declined much faster (Supplementary Fig. 5). Moreover, POC stock declined more sharply with increasing MAT in cold regions (MAT <0 °C) than in temperate (MAT >0 °C) and warm regions (MAT >15 °C), whereas MAOC stock decreased at a similar rate across different climatic regions (Supplementary Fig. 5).

Scaling up

To map the global distribution of POC and MAOC stocks, we used RF models to extrapolate our data. The model scaled up POC and MAOC stocks on a 0.5° grid while accounting for all key environmental predictors (Supplementary Table 2). Model outputs revealed that high-latitude soils contain greater POC (9.46 ± 0.05 kg m^{-2}) and MAOC (7.78 ± 0.02 kg m^{-2}) stocks, along with a higher f_{POC} ($55 \pm 0.1\%$), compared to lower-latitude soils (Supplementary Fig. 6a–c). Among land cover types, tundra soils had the highest POC stock (9.90 ± 0.04 kg m^{-2}), MAOC stock (7.91 ± 0.01 kg m^{-2}), and f_{POC} ($56 \pm 0.07\%$; Supplementary Fig. 6b, d, and f). Predicted POC and MAOC stocks were slightly higher than the measured values in our database, likely reflecting the uneven spatial distribution of observations.

To project future POC and MAOC under climate change, we used the trained RF models with future climatic predictors derived from three SSPs (SSP126, SSP245, SSP585; Fig. 3 and Supplementary Figs. 7 and 8). We quantified POC and MAOC changes as the difference between current and projected future POC and MAOC stocks (Fig. 3 and Supplementary Figs. 7 and 8). Across all climate scenarios, POC declines were substantially larger than those of MAOC, with the greatest POC losses occurring in high-latitude soils (Fig. 3h, n and Supplementary Figs. 7 and 8). Specifically, projected POC losses in high-latitude soils reached 2.67 ± 0.03, 3.59 ± 0.04, and 3.82 ± 0.05 kg m^{-2} under SSP126, SSP245, and SSP585, respectively, representing $75 \pm 3\%$, $78 \pm 11\%$, and $81 \pm 10\%$ of total predicted SOC losses (Supplementary Figs. 9–11).

Within high-latitude regions, tundra and boreal forest soils emerged as hotspots of POC losses. In tundra soils, we estimated POC losses of 2.21 ± 0.08, 3.75 ± 0.09, and 3.97 ± 0.10 kg m^{-2} under SSP126, SSP245, and SSP585, respectively, accounting for $83 \pm 7\%$, $84 \pm 9\%$, and $89 \pm 5\%$ of predicted total SOC losses (Fig. 3c, i, o and Supplementary Figs. 7 and 8). Similarly, in boreal forests, POC losses were 1.60 ± 0.02, 1.86 ± 0.03, and 1.91 ± 0.03 kg m^{-2} under the same scenarios, comprising $76 \pm 2\%$, $80 \pm 3\%$, and $85 \pm 2\%$ of total SOC losses (Supplementary Figs. 12–14). In contrast, no clear pattern was observed for MAOC, with a slight overall increase of 0.12 ± 0.01 kg m^{-2} under SSP585 (Fig. 3m–o and Supplementary Figs. 7 and 8).

To evaluate the consistency of our findings, we compared the RF model results with those from three additional machine learning algorithms: generalized boosted regression, extreme gradient boosting, and generalized linear models. All approaches consistently indicated that SOC losses in high-latitude soils are primarily driven by POC declines (Supplementary Figs. 15–17). The ensemble mean of the four models further indicates that POC losses in high-latitude soils account for $58 \pm 3\%$, $64 \pm 3\%$, and $71 \pm 5\%$ of SOC losses under SSP126, SSP245, and SSP585, respectively (Supplementary Figs. 18–20). Furthermore, when the RF model was trained exclusively on high-latitude soils, POC losses accounted for approximately $75 \pm 3\%$ of SOC losses under SSP585. This closely matched results from the full dataset, thereby underscoring the robustness of our conclusions (Supplementary Fig. 21).

While RF models are effective for large-scale extrapolation, they have limited capacity to address confounding variables and to represent biogeochemical mechanisms underlying SOC dynamics[32]. Moreover, relationships between SOC and environmental drivers may shift

https://doi.org/10.1038/s41467-026-71321-2

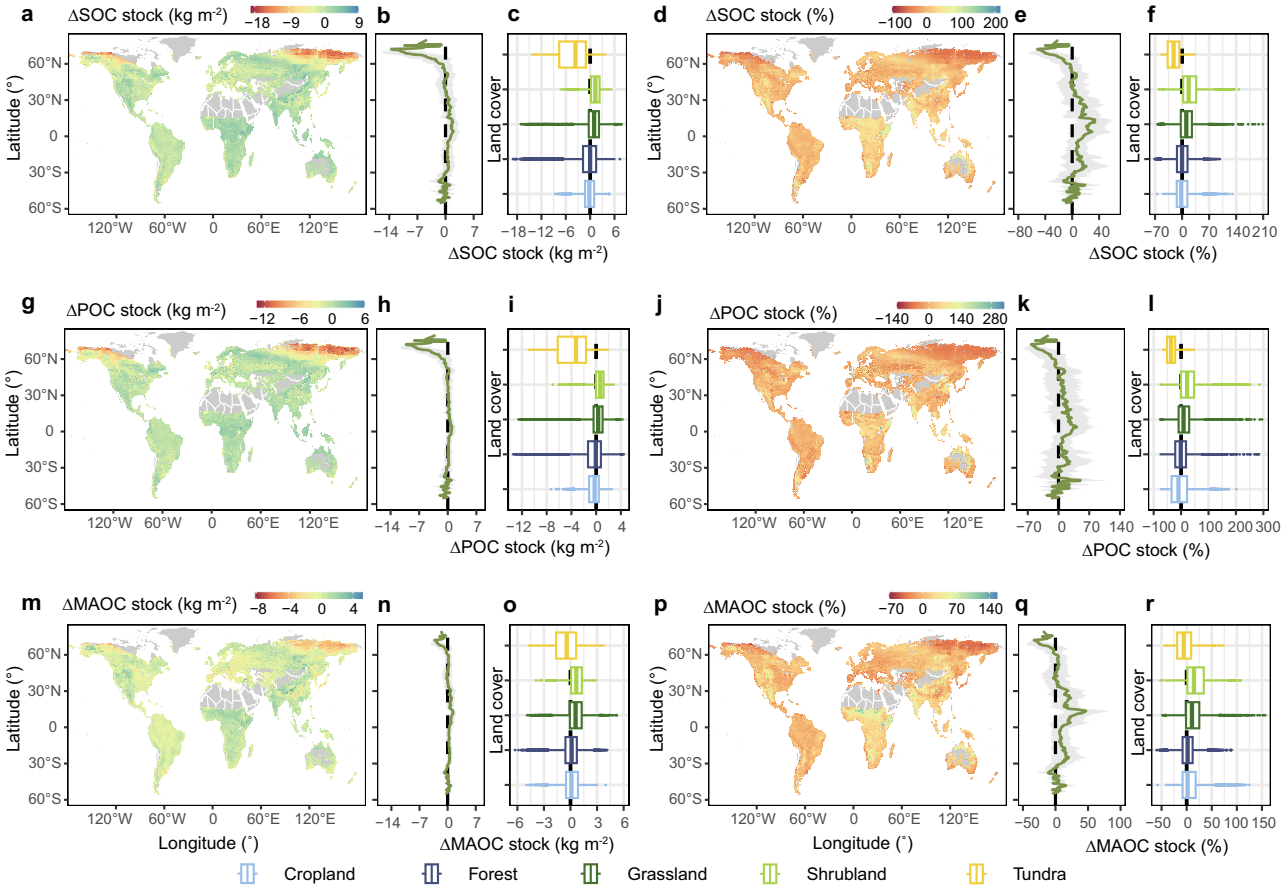

Fig. 3 | Global changes in soil organic carbon (SOC) stock, particulate organic carbon (POC) stock, and mineral-associated organic carbon (MAOC) stock under SSP 585 scenario. a, **d**, **g**, **j**, **m**, **p** Global distribution of the absolute and relative change of topsoil SOC, POC, and MAOC stocks under SSP585 scenario from 2081 to 2100. SSP, shared socioeconomic pathway. Here, SOC stock represents the sum of POC and MAOC stocks. ΔPOC, ΔMAOC, and ΔSOC stocks are the differences between the future and present stocks. The POC and MAOC stocks from 2081 to 2100 were calculated using climatic factors of different models under SSP585 scenario. The future mean annual temperature, mean annual precipitation, temperature seasonality, precipitation seasonality, evapotranspiration, and leaf area index were the means of BCC-CSM2-MR, MPI-ESM1-2-HR, and IPSL-CM6A-LR. The future nitrogen deposition background was the mean of ACCESS-ESM1-5, NorESM2-LM, and NorESM2-MM. The future net primary productivity was the mean of IPSL-CM6A-LR, CMCC-ESM2, and CanESM5-1. All maps were at 0.5° resolution. **b**, **e**, **h**, **k**, **n**, **q** Latitudinal profiles of SOC stock, POC stock, and MAOC stock change at 0.5° latitudinal resolution. The green lines represent the absolute or relative change of SOC stock, POC stock, and MAOC stock. The grey shading represents the standard deviation. **c**, **f**, **i**, **l**, **o**, **r** The absolute and relative change of SOC stock, POC stock, and MAOC stock between land covers.

under future climate and land cover changes (Luo et al., 2021), which RF models cannot explicitly capture. Thus, to further validate our findings, we used the Biogeochemistry-Informed Neural Network (BINN) model[33], using the same global POC and MAOC distributions as in our RF approach (see "Methods"). The BINN model integrates process-based biogeochemical principles (i.e., Community Land Model version 5 dynamics) with neural networks, directly recovering interpretable SOC mechanisms such as decomposition kinetics. This approach improves extrapolation robustness and reduces uncertainties in carbon cycle predictions[33]. Predictions from the BINN model confirmed the global hotspots of POC losses in high-latitude soils (Supplementary Fig. 22), adding robustness to our results.

Discussion

RF models indicate that high-latitude soils will experience significant POC losses, contributing up to 81 ± 10% of predicted total SOC losses in these regions under high-emission scenarios (SSP585; Fig. 3b, h). These projections, supported by the BINN model that integrates process-based carbon cycling biogeochemical principles with neural networks, highlight the critical role of POC losses in driving overall SOC decline (Supplementary Fig. 22). The predicted total SOC losses in high-latitude soils align with previous modeling studies[34,35], while our analysis highlights the pivotal role of POC losses in driving overall SOC declines.

MAT emerged as a key factor controlling POC and MAOC stocks (Fig. 2a, b and Supplementary Fig. 1). In cold regions, POC declined much more steeply with increasing MAT than MAOC (Supplementary Fig. 5), indicating greater temperature sensitivity of POC. This interpretation is supported by studies directly comparing POC and MAOC losses under climate change. For instance, Liu et al. found substantial POC losses due to warming-induced permafrost thaw, while MAOC remained relatively stable[36]. Similarly, Qin et al. demonstrated stronger temperature sensitivity of POC decomposition than MAOC in fraction-specific incubation experiments[37]. The steeper decline of POC with rising MAT in high-latitude soils compared to mid- and low-latitude soils further underscores the greater temperature sensitivity of POC in these regions (Supplementary Fig. 23). This pattern likely reflects that cold-adapted microbial communities respond disproportionately to even minor increases in temperature[38]. Thus, warming is expected to stimulate SOC decomposition more strongly in high-latitude soils, preferentially targeting readily accessible POC[36,39]. Furthermore, warming has more profound effects on soil extracellular enzyme activities in high-latitude soils compared to low-latitude soils, further accelerating the degradation of POC and SOC[40,41]. The relatively high

proportion of POC (f_{POC} = 55 ± 0.1%) in these soils likely amplifies this vulnerability, contributing to accelerated SOC loss under warming (Supplementary Fig. 2)[39,42].

Land cover also emerged as a key driver of POC distribution (Fig. 2a). Tundra soils contain larger POC stock and higher f_{POC} than other land covers, leading to the predicted substantial losses of POC and SOC under climate change (Fig. 3c, i and Supplementary Figs. 3, 7, and 8). This finding suggests that the abundance of POC in tundra soils could amplify SOC vulnerability, supporting emerging evidence of substantial SOC losses in tundra[29,43]. Tundra soils have historically accumulated large amounts of partially decomposed plant detritus due to low temperatures, excess soil moisture, and oxygen limitations[44,45], resulting in POC-rich organic matter[27]. The dominance of POC provides readily accessible substrates that can stimulate microbial activity under climate change, making total SOC in tundra soils more vulnerable than previously expected[27,46].

Besides tundra, forests are also projected to contribute substantially to future POC losses under climate change (Fig. 3i and Supplementary Figs. 7 and 8), with boreal forests emerging as another hotspot of POC loss (Supplementary Figs. 12–14), consistent with Lugato et al.[42] In boreal forest soils, plant inputs rich in tannins, waxes, and lignin hamper microbial metabolism[47,48], leading to greater POC accumulation and higher f_{POC} compared to temperate and tropical forest soils. However, a considerable fraction of this POC is unprotected by aggregates, making it more accessible to microbes and more susceptible to decomposition under climate change[49]. The high f_{POC} in boreal forest soils increases their vulnerability to carbon loss, as this relatively labile and weakly protected fraction is sensitive to climate-driven decomposition.

Our finding that higher f_{POC} makes SOC more vulnerable under climate change is supported by the positive correlation between f_{POC} and predicted SOC losses by 2100 across the three SSP scenarios (Fig. 4a–c). The absence of physicochemical stabilization mechanisms leaves SOC in high-f_{POC} soils more exposed to environmental perturbations[13], reinforcing the link between POC dominance and climate-driven SOC loss. In addition, the abundance of readily decomposable organic substrates in such soils facilitates faster carbon turnover, thereby amplifying SOC decomposition under climate change[50]. These mechanisms likely contribute to the strong positive carbon-climate feedback observed in high-latitude soils, where SOC is dominated or co-dominated by POC[27]. Given the greater temperature sensitivity of POC relative to MAOC, our results suggest that the dominance of POC will likely render the total SOC in high-latitude soils more vulnerable than expected under climate change. The significant correlation between f_{POC} and SOC changes in high-latitude soils further highlights f_{POC} as a valuable diagnostic tool for identifying global hotspots of SOC vulnerability (Supplementary Fig. 24) and for targeting SOC stabilization efforts.

The projected loss of POC was converted to CO_2-equivalent (CO_2e) emissions based on the CO_2/C weight ratio, highlighting the potential vulnerability of POC. Under SSP585, POC losses are estimated to generate a potential CO_2 debt of 119.96 Pg CO_2e in high-latitude soils and 81.34 Pg CO_2e globally by 2100 (Supplementary Tables 3–5), equivalent to approximately two to three times the current annual anthropogenic CO_2 emissions (41.6 Gt CO_2 yr^{-1})[2]. These results highlight the urgent need to protect POC for long-term SOC sequestration and to avoid exacerbating the climate crisis. Because POC is relatively labile and more sensitive to climatic drivers such as temperature and moisture, excluding it from model frameworks could lead to systematic underestimation of soil-derived CO_2 emissions. However, most global carbon models either treat SOC as a single homogeneous pool or emphasize the stabilization of MAOC[51]. Without accounting for the rapid turnover and large stock of POC, these models may underestimate the vulnerability of SOC under climate change, thereby biasing projections of future carbon-climate feedbacks.

Our results reveal substantial regional variation in projected POC losses under future climate scenarios, emphasizing region-specific risks under climate change (Fig. 3g, h, i and Supplementary Figs. 7 and 8). However, current model frameworks do not explicitly account for these regional differences and their critical roles in shaping SOC dynamics[52,53]. Although some models (e.g., the Microbial Efficiency-Matrix Stabilization framework 2.0 and the Millennial V2) recognize the importance of MAOC[54,55], they do not explicitly capture the temperature sensitivity of global-scale POC decomposition and its driving factors. Our analysis demonstrates that POC is markedly more temperature-sensitive in high-latitude soils than in mid- and low-latitude soils, with temperature and precipitation seasonality as well as elevation acting as key regulators (Supplementary Figs. 23 and 25). To improve predictions of SOC response to climate change, future model frameworks should integrate the spatially and temporally dynamic sensitivity of POC decomposition. In particular, recalibrating kinetic parameters, such as the regional temperature sensitivity of POC decomposition, will enhance the realism and predictive power of future climate projections[39].

Our findings highlight the importance of protecting POC to enhance SOC sequestration and stability. Historically, SOC stabilization efforts have focused on MAOC due to its long-term persistence[25,26]. However, recent studies suggest that prioritizing

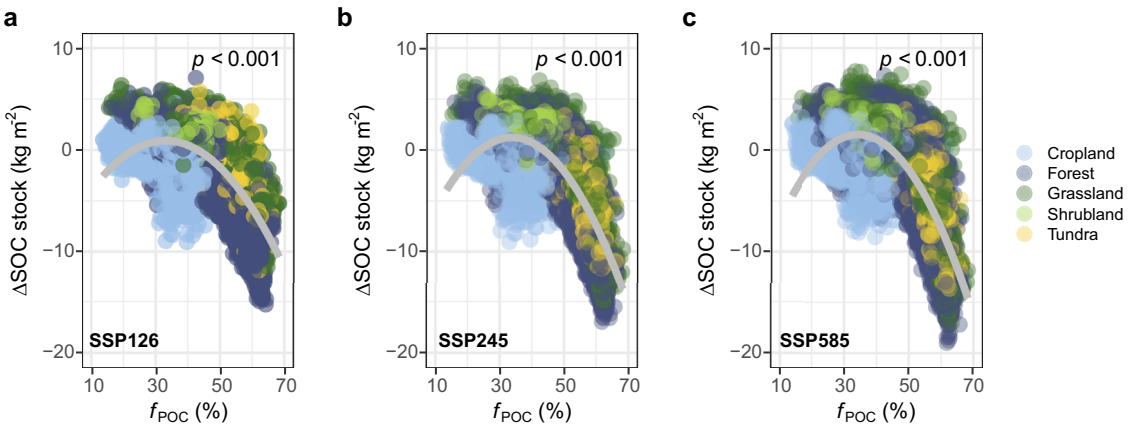

Fig. 4 | Relationship between the predicted proportion of particulate organic carbon relative to soil organic carbon (f_{POC}) and the absolute change of soil organic carbon (SOC) stock under different climate scenarios from 2081 to 2100. a–c SSP126, SSP245, and SSP585 scenarios, respectively. SSP shared socioeconomic pathway. ΔSOC stock is the difference between the future and present SOC stock. Different colors of points represent the various land covers.

MAOC alone is insufficient for enhancing SOC stock[30,56]. Thus, soil management strategies for enhancing SOC sequestration should also focus on increasing and preserving POC. For instance, in forest soils where POC contributes more to SOC than MAOC, management practices targeting only MAOC did not increase total SOC stocks[57]. In contrast, forest management practices that enhance POC stock, such as restoring biodiversity or retaining more plant residues (e.g., leaves and branches), can significantly improve SOC sequestration[58–60]. In addition, our projections show that future climate change will lead to substantial POC losses, while reductions in MAOC are comparatively minor or even reversed in mid- and low-latitude soils. This suggests that simultaneously protecting POC and promoting its transformation into MAOC can jointly enhance SOC stability. For example, conservation practices such as regenerative agriculture, cover crop planting, and straw return have already been shown to increase both POC and SOC stocks in cropland soils by enhancing carbon inputs and reducing soil disturbance[61,62]. Collectively, these findings underscore the need to protect and enhance both POC and MAOC as equally critical pathways for SOC sequestration and long-term stability.

While our results provide globally applicable insights, some limitations of our analysis should be noted. First, a mismatch may exist between the POC and MAOC observations and the environmental variables extracted from global databases. Although all variables were standardized to a 0.5° resolution and aligned with each sampling site, differences in the temporal coverage of SOC fraction measurements and environmental data may introduce additional uncertainty. Second, agricultural management practices, such as tillage, fertilization, and residue retention, substantially alter SOC dynamics, especially in croplands[62]. This is an important source of uncertainty, and future work should incorporate management-specific datasets to refine predictions of POC and MAOC under changing climate conditions. Third, we currently have a limited understanding of how occluded and free POC respond to climate change. Because occluded POC is physically protected within aggregates, it may exhibit lower temperature sensitivity than free POC[8], emphasizing the need for more empirical observations.

Our study underscores the pivotal role of land cover and temperature in shaping global POC and MAOC distributions. Tundra and boreal forest soils emerge as global hotspots for POC losses under climate change, driven by high f_{POC} and lower temperatures. The losses of POC account for 81 ± 10% of the projected SOC declines for high-latitude soils under SSP585, emphasizing the need to incorporate POC protection into SOC stabilization strategies. By leveraging this global dataset, we highlight the necessity of integrating POC dynamics into future research and conservation efforts to enhance SOC resilience under climate change.

Methods

Data compilation

We systematically collected peer-reviewed articles before August 2024 that measured POC and MAOC content or stock by searching Google Scholar (http://scholar.google.com/), Web of Science (http://apps.webofknowledge.com/), and China National Knowledge Infrastructure (http://www.cnki.net). The keywords and phrases used for literature research were as follows: (i) "POC" or "Particulate organic matter" or "Light fraction"; (ii) "MAOC" or "Mineral associated organic matter" or "heavy fraction"; and (iii) "soil" or "land" or "terrestrial". The following criteria were used to screen the data for this study: (1) POC and MAOC must be obtained by dispersing bulk soil; (2) the data collected must be measured in mineral soil horizons; (3) only POC or MAOC from topsoil (0–30 cm) was collected. Previous databases on POC and MAOC[18,24,25,27,42,63–67] were incorporated into our dataset. To include as many reliable observations as possible, we contacted scientists across the world working in this research area for their data contribution. In addition, the 200 observations from Australia in our database were obtained through spectroscopic modeling based on infrared methods[68]. SOC fractionation based on particle size (POC higher than 50–63 µm), density, or both particle size and density (POC lighter than 1.60–1.85 g cm^{-3}) were included in the database, as they give similar results in comparative studies (Supplementary Notes). The final database comprised 3284 observations (560 unpublished), which included soil fractions by particle size (n = 2484), density (n = 390), or the combination of particle size and density (n = 410; Supplementary Notes).

To investigate the influence of environmental factors on POC and MAOC, we selected 16 variables that represent major drivers of SOC dynamics (Supplementary Table 2). All variables were resampled to a uniform spatial resolution of 0.5°. When results were presented graphically, we used Engauge Digitizer (https://digitizer.sourceforge.net/) to digitize the data. To obtain geographical coordinates for data points where such information was not reported, we conducted a search using the names of the sites, states, and countries. These coordinates were then used to map sites globally (Fig. 1a) and extract missing data from global databases. We obtained MAT, MAP, temperature seasonality, and precipitation seasonality from the WorldClim Database[69]. Potential evapotranspiration was obtained from the GLEAM v3 database[70]. The ratio of potential evapotranspiration to MAP represented the aridity index. Background nitrogen deposition was retrieved from the Global Nitrogen Deposition database[71], while net primary productivity and mean leaf area index came from the MOD17A3HGF product (https://lpdaac.usgs.gov/products/mod17a3hgfv006) and Cao et al.[72], respectively. Soil pH and soil texture were obtained from the Harmonized World Soil Database[73]. Soil cation exchange capacity was obtained from the SoilGrids database[74] and soil total phosphorus from ref. 75. In addition, soil was classified into low- or high-activity minerals based on clay composition and soil order data from each study[25,76]. We chose these open-access resources for their global coverage, relatively high spatial resolution, and widespread recognition in soil and ecosystem research. As the climatic variables represent multi-year averages and SOC typically changes slowly, any temporal mismatches among datasets are expected to have minimal impact relative to spatial variability[77].

Overview of the database and data quality control

Compared with previous global datasets, our dataset is more comprehensive and includes unpublished data. The database represented almost all geographical regions and climatic regions, spanning a wide range of MAP (9.05 to 5000 mm yr^{-1}) and MAT (−13.5 to 30.0 °C; Fig. 1a, b). Terrestrial land covers in the database included cropland (n = 1165), forest (n = 1135), grassland (n = 693), shrubland (n = 262), and tundra (n = 29). By applying strict quality-control criteria during data screening, we improved the reliability of POC and MAOC. To be included in our dataset, all data had to meet the following quality criteria: (1) SOC recovery percent (i.e., the sum of POC and MAOC stocks as a percentage of total SOC stock) should range from 80 to 120%; (2) the contributions of POC and MAOC to SOC should be lower than 95% and higher than 5%, respectively; and (3) selected publications should clearly describe their the methodology employed, including the specific steps of fractional calculations and appropriate references to the adopted methodologies. These criteria were established to account for potential errors introduced during the fractionation and measurement processes, ensuring the internal consistency and reliability of the compiled dataset. In total, 489 observations that failed to meet these quality criteria were excluded from the final database.

Soil sampling depths are highly varied across different studies. To enhance the comparability of POC and MAOC from various studies, we adopted the methodology of Jobbágy and Jackson[78], as modified by McClelland et al.[79], to standardize observed values to a uniform soil

depth of 0–30 cm using the following equation:

$$POC_{30} = \frac{1-\beta^{30}}{1-\beta^{dx}} \times POC_{dx} \quad (1)$$

$$MAOC_{30} = \frac{1-\beta^{30}}{1-\beta^{dx}} \times MAOC_{dx} \quad (2)$$

where POC_{30} and $MAOC_{30}$ represent the value of POC and MAOC in kg C m^{-2} within the uppermost 30 cm of the soil profile. The parameter β represents the relative reduction rate of SOC pools with increasing soil depth across different land covers (Supplementary Fig. 26). The β values for different land covers were calculated following the methodology adapted from Jobbágy and Jackson[78]. Utilizing global SOC (0–20 cm) from SoilGrids (https://www.isric.org/explore/soilgrids), we developed linear regression equations to establish the relationship between SOC stock and soil depth. Based on these relationships, we simulated the SOC distribution across the 0–30 cm soil profile and subsequently quantified the β. The variable dx denotes the original soil depth recorded in individual studies (cm), and POC_{dx} and $MAOC_{dx}$ are the original stocks of POC and MAOC, respectively.

Data analyses

We predicted global POC and MAOC stocks using four machine learning models: RF, generalized boosted regression, extreme gradient boosting, and generalized linear models. Among these, the RF model is based on decision tree bagging, while the generalized boosted regression and extreme gradient boosting models are based on decision tree boosting approaches. The generalized linear model represents a standard linear regression approach. Predictors included MAT, MAP, elevation, temperature seasonality, precipitation seasonality, aridity index, land cover, net primary productivity, leaf area index, clay + silt content, soil cation exchange capacity, soil pH, and soil mineral activity for MAOC stock (Supplementary Table 2). Prior to modeling, we tested for multicollinearity and ensured all variables had variance inflation factors below five[80]. To assess model robustness and potential overfitting, we generated learning curves to examine model performance as a function of training data proportion (Supplementary Fig. 27). The dataset was ultimately split into training (80%) and test (20%) sub-data sets.

To ensure model robustness, we performed hyperparameter tuning for each method. RF model optimization focused on two hyperparameters: the number of variables randomly sampled at each split (mtry) and the number of trees (ntree). We conducted a grid search across mtry ranging from 2 to 13 in steps of 2, and ntree ranging from 300 to 1500 in increments of 100. Generalized boosted regression model optimization was based on a parameter grid combining the number of trees (200–1200), interaction depth (1, 3, and 5), learning rate (0.01–0.10), and minimum number of observations per terminal node (5 or 10). Extreme gradient boosting model optimization was performed using a grid search across key hyperparameters, including the number of boosting rounds (50–300, with increments of 50), maximum tree depth (2, 3, 4, and 5), learning rate (0.05, 0.1, and 0.2), minimum loss reduction required for further partitioning (gamma = 0 or 0.1), column subsampling rate for each tree (0.8 and 1), minimum child weight (1 and 3), and the subsampling ratio of the training data (0.8 and 1). Generalized linear model optimization used a tuning length of 30 to systematically evaluate regularization parameters across both ridge and lasso penalties. For each parameter combination, model performance was assessed through five-fold cross-validation implemented in the caret package. Based on these evaluations, RF model exhibited the highest predictive accuracy, as indicated by the lowest root mean square error (RMSE) and the highest coefficient of determination (R^2), and was therefore selected for the final predictions of POC and MAOC stocks (Supplementary Fig. 28).

We used the RF models to predict POC stock, MAOC stock, and f_{POC}, as well as to identify their key predictors. The RF models were retrained using the best parameter set on the training dataset and subsequently evaluated against the independent test dataset (Supplementary Fig. 28). Variable importance was quantified using the permutation-based increase in mean squared error (%IncMSE)[81]. The RF models explained 54%, 64%, and 63% of the variance in POC stock, MAOC stock, and f_{POC}, respectively. RMSE values were 2.40 kg m^{-2} for POC stock, 2.57 kg m^{-2} for MAOC stock, and 12% for f_{POC} (Supplementary Fig. 28). We then estimated the present global distribution of POC stock, MAOC stock, and f_{POC} based on these RF models (Supplementary Figs. 6 and 29). The gridded variables used for the global predictions were all re-gridded to a spatial resolution of 0.5° × 0.5°.

To project changes in POC and MAOC stocks under future climate scenarios, we used climate model outputs for the period 2081–2100 under three representative SSPs (SSP126, SSP245, and SSP585)[82]. This period aligns with the long-term projections defined in the IPCC Sixth Assessment Report, which assesses climate change relative to the 1850–1900 baseline. Using this timeframe allows for a robust evaluation of carbon stock responses under stabilized future climate conditions and facilitates comparison with previous studies and IPCC projections. These scenarios capture a broad range of plausible futures: SSP126 reflects a sustainable, low-emission pathway with stringent mitigation policies, SSP245 represents an intermediate "middle-of-the-road" trajectory with moderate mitigation efforts, and SSP585 depicts a high-emission scenario with minimal climate intervention.

Future climate variables included MAT, MAP, temperature seasonality, precipitation seasonality, background nitrogen deposition, net primary productivity, potential evapotranspiration, and leaf area index. The aridity index was calculated as the ratio of potential evapotranspiration to MAP. Data for future MAT, MAP, temperature seasonality, and precipitation seasonality were obtained from the WorldClim repository[69], while future background nitrogen deposition, net primary productivity, potential evapotranspiration, and leaf area index were sourced from the World Climate Research Programme's CMIP6 database (https://esgf-node.ipsl.upmc.fr/projects/cmip6-ipsl/). Future land cover was obtained from the global land-use and land-cover change (LUCC) simulation product[83]. All shrubland situated north of 60°N was considered as tundra. We applied the trained RF models to these future climate scenarios to predict POC stock, MAOC stock, and f_{POC} (Supplementary Figs. 29–35). Future SOC stock was calculated as the sum of future POC and MAOC stocks. By analyzing changes in SOC, POC, MAOC, and f_{POC}, we assessed SOC vulnerability under projected climate conditions. We converted the projected SOC losses under the SSP126, SSP245, and SSP585 scenarios into CO_2e emissions using the molecular weight ratio between carbon and CO_2. Specifically, the SOC, MAOC, or POC loss was multiplied by 44/12, corresponding to the molecular weight of CO_2 (44 g mol^{-1}) relative to carbon (12 g mol^{-1}), to obtain the equivalent CO_2 emissions (Supplementary Tables 3–5).

To evaluate the robustness of our results, we conducted a series of sensitivity analyses using subsets of the dataset. First, we developed separate RF models for high-latitude soils, using the same environmental predictors and hyperparameter optimization as in the global models, to predict present and future POC and MAOC stocks under different climate scenarios (Supplementary Fig. 21). Second, we separately developed models for each methodological category in the compiled dataset to generate independent predictions of POC and MAOC (Supplementary Figs. 36–38). Third, to account for potential biases introduced by standardizing SOC fractions to a uniform depth of 0–30 cm, we also trained models on the original, non-homogenized data. Predictions from these parallel analyses were compared with the

main results to assess the consistency and reliability of our findings (Supplementary Fig. 39).

The BINN model was used to predict POC and MAOC stocks under the SSP245 scenario by integrating process-based biogeochemical modeling with neural networks (Supplementary Methods)[33]. The model first processed environmental covariates (e.g., temperature, precipitation, soil properties) using a fully connected neural network. The neural network's predicted parameters were then incorporated into CLM5, where POC was derived from the "fast" pool and MAOC from the "slow" and "passive" pools. For scenario projections, the trained BINN model estimated POC and MAOC stocks (0–30 cm) under SSP245 forcings, using neural networks to generalize parameter-environment relationships.

The normality of each variable was tested using the Shapiro–Wilk test[84], which indicated that POC stock, MAOC stock, and f_{POC} did not follow a normal distribution. To analyze differences across land cover types, forest types, and latitude regions, we used the Kruskal–Wallis test. To investigate the temperature responses of POC, MAOC, and f_{POC}, we applied segmented linear regressions to examine their relationships with MAT across cold (<0°C), temperate (≥0 °C and <15°C), and warm (≥15 °C) regions. Additionally, quadratic polynomial models were fitted to capture potential non-linear patterns of POC and MAOC with MAT. Coefficients from the polynomial models were then used to calculate point-specific slopes (first derivatives). These slopes quantify the rate of change in POC and MAOC stocks with increasing MAT. RF models were subsequently employed to identify the key environmental drivers underlying spatial variations in the POC slopes. All analyses were conducted in R version 4.1.0 (R Core Team, 2021), and figures were generated using the ggplot2 package[85].

Data availability

The data used in this study are available online in the Figshare database (https://figshare.com/s/501e92df94a15ae4ebfe).

Code availability

The analysis code that supports the findings of this study is available on Figshare (https://figshare.com/s/501e92df94a15ae4ebfe).

References

1. Amelung, W. et al. Towards a global-scale soil climate mitigation strategy. *Nat. Commun.* **11**, 5427 (2020).
2. Friedlingstein, P. et al. Global carbon budget 2024. *Earth Syst. Sci. Data* **17**, 965–1039 (2025).
3. Kopittke, P. M. et al. Ensuring planetary survival: the centrality of organic carbon in balancing the multifunctional nature of soils. *Crit. Rev. Environ. Sci. Technol.* **52**, 4308–4324 (2022).
4. Lal, R. Soil carbon sequestration impacts on global climate change and food security. *Science* **304**, 1623–1627 (2004).
5. Tiessen, H., Cuevas, E. & Chacon, P. The role of soil organic matter in sustaining soil fertility. *Nature* **371**, 783–785 (1994).
6. Beillouin, D. et al. A global meta-analysis of soil organic carbon in the Anthropocene. *Nat. Commun.* **14**, 3700 (2023).
7. Garsia, A., Moinet, A., Vazquez, C., Creamer, R. E. & Moinet, G. Y. K. The challenge of selecting an appropriate soil organic carbon simulation model: a comprehensive global review and validation assessment. *Glob. Change Biol.* **29**, 5760–5774 (2023).
8. Lavallee, J. M., Soong, J. L. & Cotrufo, M. F. Conceptualizing soil organic matter into particulate and mineral-associated forms to address global change in the 21st century. *Glob. Change Biol.* **26**, 261–273 (2020).
9. Jackson, R. B. et al. The ecology of soil carbon: pools, vulnerabilities, and biotic and abiotic controls. *Annu. Rev. Ecol. Evol. Syst.* **48**, 419–445 (2017).
10. Cotrufo, M. F. & Lavallee, J. M. Soil organic matter formation, persistence, and functioning: a synthesis of current understanding to inform its conservation and regeneration. *Adv. Agron.* **172**, 1–66 (2022).
11. Whalen, E. D. et al. Clarifying the evidence for microbial- and plant-derived soil organic matter, and the path toward a more quantitative understanding. *Glob. Change Biol.* **28**, 7167–7185 (2022).
12. Cotrufo, M. F. et al. Formation of soil organic matter via biochemical and physical pathways of litter mass loss. *Nat. Geosci.* **8**, 776–779 (2015).
13. von Lützow, M. et al. SOM fractionation methods: relevance to functional pools and to stabilization mechanisms. *Soil Biol. Biochem.* **39**, 2183–2207 (2007).
14. Guggenberger, G., Zech, W., Haumaier, L. & Christensen, B. T. Land-use effects on the composition of organic matter in particle-size separates of soils: II. CPMAS and solution ^{13}C NMR analysis. *Eur. J. Soil Sci.* **46**, 147–158 (1995).
15. Kleber, M. et al. Chapter one - mineral–organic associations: formation, properties, and relevance in soil environments. *Adv. Agron.* **130**, 1–140 (2015).
16. Villarino, S. H., Pinto, P., Jackson, R. B. & Piñeiro, G. Plant rhizodeposition: a key factor for soil organic matter formation in stable fractions. *Sci. Adv.* **7**, eabd3176 (2021).
17. Christensen, B. T. Physical fractionation of soil and organic matter in primary particle size and density separates. *Adv. Soil Sci.* **20**, 1–90 (1992).
18. Heckman, K. et al. Beyond bulk: density fractions explain heterogeneity in global soil carbon abundance and persistence. *Glob. Change Biol.* **28**, 1178–1196 (2022).
19. Lobe, I., Sandhage-Hofmann, A., Brodowski, S., du Preez, C. C. & Amelung, W. Aggregate dynamics and associated soil organic matter contents as influenced by prolonged arable cropping in the South African Highveld. *Geoderma* **162**, 251–259 (2011).
20. Six, J., Bossuyt, H., Degryze, S. & Denef, K. A history of research on the link between (micro)aggregates, soil biota, and soil organic matter dynamics. *Soil Tillage Res* **79**, 7–31 (2004).
21. Six, J., Elliott, E. T. & Paustian, K. Soil macroaggregate turnover and microaggregate formation: a mechanism for C sequestration under no-tillage agriculture. *Soil Biol. Biochem.* **32**, 2099–2103 (2000).
22. Willard, S. J. et al. Land use drives the distribution of free, physically protected, and chemically protected soil organic carbon storage at a global scale. *Glob. Change Biol.* **30**, e17507 (2024).
23. Zhang, Z. et al. Short-term warming supports mineral-associated carbon accrual in abandoned croplands. *Nat. Commun.* **16**, 344 (2025).
24. Díaz-Martínez, P. et al. Vulnerability of mineral-associated soil organic carbon to climate across global drylands. *Nat. Clim. Change* **14**, 976–982 (2024).
25. Georgiou, K. et al. Global stocks and capacity of mineral-associated soil organic carbon. *Nat. Commun.* **13**, 3797 (2022).
26. Zhou, Z. et al. Global turnover of soil mineral-associated and particulate organic carbon. *Nat. Commun.* **15**, 5329 (2024).
27. García-Palacios, P. et al. Dominance of particulate organic carbon in top mineral soils in cold regions. *Nat. Geosci.* **17**, 145–150 (2024).
28. Mueller, C. W. & Koegel-Knabner, I. Soil organic carbon stocks, distribution, and composition affected by historic land use changes on adjacent sites. *Biol. Fertil. Soils* **45**, 347–359 (2009).
29. Prater, I. et al. From fibrous plant residues to mineral-associated organic carbon – the fate of organic matter in Arctic permafrost soils. *Biogeosciences* **17**, 3367–3383 (2020).
30. Angst, G. et al. Unlocking complex soil systems as carbon sinks: multi-pool management as the key. *Nat. Commun.* **14**, 2967 (2023).
31. Janzen, H. H. Russell review soil carbon stewardship: thinking in circles. *Eur. J. Soil Sci.* **75**, e13536 (2024).
32. Reichstein, M. et al. Deep learning and process understanding for data-driven Earth system science. *Nature* **566**, 195–204 (2019).

33. Xu, H. et al. Biogeochemistry-informed neural network (BINN) for improving accuracy of model prediction and scientific understanding of soil organic carbon. Preprint at https://arxiv.org/abs/2502.00672 (2025).
34. McGuire, A. D. et al. Dependence of the evolution of carbon dynamics in the northern permafrost region on the trajectory of climate change. *Proc. Natl. Acad. Sci. USA* **115**, 3882–3887 (2018).
35. Mekonnen, Z. A. et al. Wildfire exacerbates high-latitude soil carbon losses from climate warming. *Environ. Res. Lett.* **17**, 094037 (2022).
36. Liu, F. et al. Divergent changes in particulate and mineral-associated organic carbon upon permafrost thaw. *Nat. Commun.* **13**, 5073 (2022).
37. Qin, S. et al. Linkage between temperature sensitivity of SOM decomposition and microbial communities depends on soil fractions. *Glob. Change Biol.* **30**, e17456 (2024).
38. D'Alò, F. et al. Microbial activity in alpine soils under climate change. *Sci. Total Environ.* **783**, 147012 (2021).
39. Georgiou, K. et al. Emergent temperature sensitivity of soil organic carbon driven by mineral associations. *Nat. Geosci.* **17**, 205–212 (2024).
40. Pei, J., Fang, C., Li, B., Nie, M. & Li, J. Direct evidence for microbial regulation of the temperature sensitivity of soil carbon decomposition. *Glob. Change Biol.* **30**, e17523 (2024).
41. Meng, C. et al. Global meta-analysis on the responses of soil extracellular enzyme activities to warming. *Sci. Total Environ.* **705**, 135992 (2020).
42. Lugato, E., Lavallee, J. M., Haddix, M. L., Panagos, P. & Cotrufo, M. F. Different climate sensitivity of particulate and mineral-associated soil organic matter. *Nat. Geosci.* **14**, 295–300 (2021).
43. Gentsch, N. et al. Properties and bioavailability of particulate and mineral-associated organic matter in Arctic permafrost soils, Lower Kolyma Region, Russia. *Eur. J. Soil Sci.* **66**, 722–734 (2015).
44. Hicks Pries, C. E., Schuur, E. A. G. & Crummer, K. G. Holocene carbon stocks and carbon accumulation rates altered in soils undergoing permafrost thaw. *Ecosystems* **15**, 162–173 (2012).
45. Lee, H., Schuur, E. A. G., Inglett, K. S., Lavoie, M. & Chanton, J. P. The rate of permafrost carbon release under aerobic and anaerobic conditions and its potential effects on climate. *Glob. Change Biol.* **18**, 515–527 (2012).
46. van Gestel, N. et al. Predicting soil carbon loss with warming. *Nature* **554**, E4–E5 (2018).
47. Almeida, L. F. J. et al. Forest litter constraints on the pathways controlling soil organic matter formation. *Soil Biol. Biochem.* **163**, 108447 (2021).
48. Kögel-Knabner, I. & Amelung, W. Soil organic matter in major pedogenic soil groups. *Geoderma* **384**, 114785 (2021).
49. Schrumpf, M. et al. Storage and stability of organic carbon in soils as related to depth, occlusion within aggregates, and attachment to minerals. *Biogeosciences* **10**, 1675–1691 (2013).
50. Craig, M. E. et al. Fast-decaying plant litter enhances soil carbon in temperate forests but not through microbial physiological traits. *Nat. Commun.* **13**, 1229 (2022).
51. Dangal, S. R. S. et al. Improving soil carbon estimates by linking conceptual pools against measurable carbon fractions in the DAYCENT model version 4.5. *J. Adv. Model. Earth Syst.* **14**, e2021MS002622 (2022).
52. Blankinship, J. C. et al. Improving understanding of soil organic matter dynamics by triangulating theories, measurements, and models. *Biogeochemistry* **140**, 1–13 (2018).
53. Sulman, B. N., Phillips, R. P., Oishi, A. C., Shevliakova, E. & Pacala, S. W. Microbe-driven turnover offsets mineral-mediated storage of soil carbon under elevated CO_2. *Nat. Clim. Change* **4**, 1099–1102 (2014).
54. Schimel, J. Modeling ecosystem-scale carbon dynamics in soil: the microbial dimension. *Soil Biol. Biochem.* **178**, 108948 (2023).
55. Zhang, Y. et al. Simulating measurable ecosystem carbon and nitrogen dynamics with the mechanistically defined MEMS 2.0 model. *Biogeosciences* **18**, 3147–3171 (2021).
56. King, A. E. et al. Constraints on mineral-associated and particulate organic carbon response to regenerative management: carbon inputs and saturation deficit. *Soil Tillage Res.* **238**, 106008 (2024).
57. Chari, N. R. & Taylor, B. N. Soil organic matter formation and loss are mediated by root exudates in a temperate forest. *Nat. Geosci.* **15**, 1011–1016 (2022).
58. Ortiz, C. A., Lundblad, M., Lundström, A. & Stendahl, J. The effect of increased extraction of forest harvest residues on soil organic carbon accumulation in Sweden. *Biomass-. Bioenergy* **70**, 230–238 (2014).
59. Kristensen, J. Å et al. Tree planting is no climate solution at northern high latitudes. *Nat. Geosci.* **17**, 1087–1092 (2024).
60. Augusto, L. & Boča, A. Tree functional traits, forest biomass, and tree species diversity interact with site properties to drive forest soil carbon. *Nat. Commun.* **13**, 1097 (2022).
61. Liu, C., Lu, M., Cui, J., Li, B. & Fang, C. Effects of straw carbon input on carbon dynamics in agricultural soils: a meta-analysis. *Glob. Change Biol.* **20**, 1366–1381 (2014).
62. Prairie, A. M., King, A. E. & Cotrufo, M. F. Restoring particulate and mineral-associated organic carbon through regenerative agriculture. *Proc. Natl. Acad. Sci. USA* **120**, e2217481120 (2023).
63. Cotrufo, M. F., Ranalli, M. G., Haddix, M. L., Six, J. & Lugato, E. Soil carbon storage informed by particulate and mineral-associated organic matter. *Nat. Geosci.* **12**, 989–994 (2019).
64. Doetterl, S. et al. Soil carbon storage controlled by interactions between geochemistry and climate. *Nat. Geosci.* **8**, 780–783 (2015).
65. Hansen, P. M. et al. Distinct, direct and climate-mediated environmental controls on global particulate and mineral-associated organic carbon storage. *Glob. Change Biol.* **30**, e17080 (2024).
66. Sokol, N. W. et al. Global distribution, formation and fate of mineral-associated soil organic matter under a changing climate: a trait-based perspective. *Funct. Ecol.* **36**, 1411–1429 (2022).
67. Zhao, P. et al. Quantifying soil properties relevant to soil organic carbon biogeochemical cycles by infrared spectroscopy: the importance of compositional data analysis. *Soil Tillage Res* **231**, 105718 (2023).
68. Viscarra Rossel, R. A. et al. Continental-scale soil carbon composition and vulnerability modulated by regional environmental controls. *Nat. Geosci.* **12**, 547–552 (2019).
69. Fick, S. E. & Hijmans, R. J. WorldClim 2: new 1-km spatial resolution climate surfaces for global land areas. *Int. J. Climatol.* **37**, 4302–4315 (2017).
70. Martens, B. et al. GLEAM v3: satellite-based land evaporation and root-zone soil moisture. *Geosci. Model Dev.* **10**, 1903–1925 (2017).
71. ORNL DAAC. *Dataset "Bailey Ecoregions of the Continents (Province)"* https://doi.org/10.3334/ORNLDAAC/1388 (2017).
72. Cao, S. et al. Spatiotemporally consistent global dataset of the GIMMS leaf area index (GIMMS LAI4g) from 1982 to 2020. *Earth Syst. Sci. Data* **15**, 4877–4899 (2023).
73. Wieder, W. R., Boehnert, J., Bonan, G. B. & Langseth, M. Regridded Harmonized World Soil Database v1.2. Data set. *Oak Ridge Natl. Lab. Distrib. Act. Arch. Center, Oak Ridge, Tennessee, USA*. https://doi.org/10.3334/ORNLDAAC/1247 (2014).
74. Hengl, T. et al. Soil Grids 250m: global gridded soil information based on machine learning. *PLoS ONE* **12**, e0169748 (2017).
75. He, X. et al. Global patterns and drivers of soil total phosphorus concentration. *Earth Syst. Sci. Data* **13**, 5831–5846 (2021).
76. Ito, A. & Wagai, R. Global distribution of clay-size minerals on land surface for biogeochemical and climatological studies. *Sci. Data* **4**, 170103 (2017).

77. Wieder, W. R. et al. Carbon cycle confidence and uncertainty: exploring variation among soil biogeochemical models. *Glob. Change Biol.* **24**, 1563–1579 (2018).
78. Jobbágy, E. G. & Jackson, R. B. The vertical distribution of soil organic carbon and ITS relation to climate and vegetation. *Ecol. Appl.* **10**, 423–436 (2000).
79. McClelland, S. C., Paustian, K. & Schipanski, M. E. Management of cover crops in temperate climates influences soil organic carbon stocks: a meta-analysis. *Ecol. Appl.* **31**, e02278 (2021).
80. Murtagh, F. & Heck, A. *Multivariate Data Analysis* 0-236 (Springer-Verlag, Berlin, Heidelberg, 1987).
81. Grömping, U. Variable importance assessment in regression: linear regression versus random forest. *Am. Statist.* **63**, 308–319 (2009).
82. O'Neill, B. C. et al. The scenario model intercomparison project (ScenarioMIP) for CMIP6. *Geosci. Model Dev.* **9**, 3461–3482 (2016).
83. Li, X. et al. A new global land-use and land-cover change product at a 1-km resolution for 2010 to 2100 based on human–environment interactions. *Ann. Am. Assoc. Geogr.* **107**, 1040–1059 (2017).
84. Shapiro, S. S. & Wilk, M. B. An analysis of variance test for normality (complete samples). *Biometrika* **52**, 591–611 (1965).
85. Wickham, H. ggplot2: *Elegant Graphics for Data Analysis* (Springer-Verlag New York, 2009).

Acknowledgements

This study is supported by the National Natural Science Foundation of China (32471685, 42361144886) and Shaanxi Province Natural Science Foundation for Distinguished Young Scholar (2024JC-JCQN-32).

Author contributions

S.S. conceived the study together with Ji Chen. S. S. collected data from peer-reviewed articles. A.H.K., B.S., B.J.C., Chang Liao, D.G., E.H., F.Z., F.T.M., F.B., F.W., G.V.G., G.L., G.H., G.A.S., G.H.-R., G.N., G.S., I.L., J.B., J.W., K.K., K.G., L.D., L.G., M.D.-B., M.D., M.L., M.K., O.K., P.R., P.D., P.Z., R.A.V. R., R.V., R.C., R.L., S.V., S.X., S.N., S.C., T.Y., T.G., W.L., W.S., W.W., W.B., Xiangrong Cheng, X.L., X.S., Xiaoli Cheng, X.W., X.L., X.Z., Y.K., Yangquanwei Zhong, Y.C., Y.Y., Yuyi Li, Z.C., Zhanfeng Liu, and Zhongkui Luo provided their unpublished data. S.S. conducted the analyses and performed visualization, with contributions from F.T., H.X., and Yiqi Luo. S.S., Ji Chen, M.F.C., R.A.V.R., and K.J.v.G. wrote the manuscript. A.G.H., A.M., A.H.K., W.A., A.K., A.S., B.S., B. J.C., C.P., C.T., Chang Liang, Chang Liao, C.J., D.G., E.L., E.H., F.D., F.Z., F.T., F.T.M., F.B., F.W., G.V.G., G.L., G.H., G.A.S., G.H.-R., G.N., G.P., G.S., H.Z., H.A., H.X., I.L., I.K., J.B., J.Å.K., J.L., J.Z., J W., J.A., Junji Cao, J.E.O., K.K., K.G., K.V.O., K.A.F., L.D., L.G.B., L.G., L.M., M.D.-B., M.D., M.R., M.L., O.K., O.H., P.G.-P., P.H., P.R., P.D., P.Z., P.M.H., R.G., R.Ž., R.B., R.V., R.C., R.L., S.V., S.X., S.N., S.C., T.Y., S.J.H., T.K., T.G., V.E.M., V.M.S., W.L., W.S., W.Z., W.W., W.B., Xiangrong Cheng, X.L., X.S., Xiaoli Cheng, X.W., X.L., X.Z., Y.K., Yangquanwei Zhong, Y.C., Y.Y., Yiqi Luo, Yixuan Zhang, Y.Q., Y.F., Yuting Liang, Yuyi Li, Z.C., Zhanfeng Liu, Z.S., Zhongkui Luo, and Z.A. edited the manuscript. M.F.C., R.A.V.R., C.W.M., M.K., K.J.v.G., Z.A., and Ji Chen edited the manuscript and contributed to the discussion on the effects of climate change on particulate and mineral-associated organic carbon. All authors read and approved the final manuscript.

Competing interests

The authors declare no competing interests.

Additional information

Supplementary information The online version contains supplementary material available at https://doi.org/10.1038/s41467-026-71321-2.

Correspondence and requests for materials should be addressed to Ji Chen.

Peer review information *Nature Communications* thanks Carlos Eduardo Cerr and the other, anonymous, reviewer(s) for their contribution to the peer review of this work. A peer review file is available.

Siyi Sun[1,2], M. Francesca Cotrufo[3], R. A. Viscarra Rossel[4], Carsten W. Mueller[5,6], Morimaru Kida[7], Ailsa G. Hardie[8], Alec Mackay[9], Alexander H. Krichels[10,11], Wulf Amelung[12], Amit Kumar[13], Azamat Suleymanov[14,15], Baoku Shi[16], Bernard Jackson Cosby[17], César Plaza[18,19], César Terrer[20], Chang Liang[21], Chang Liao[22], Christopher Just[23], Ding Guo[24], Emanuele Lugato[25], Enqing Hou[26], Fan Ding[27], Fazhu Zhao[28], Feng Tao[29], Fernando T. Maestre[30], Franco Bilotto[31], Fuzhong Wu[32], Gisela V. García[33], Gongwen Luo[34], Guangxuan Han[35], Guillermo A. Studdert[33], Guillermo Hernandez-Ramirez[36], Guoxiang Niu[26], Gervasio Piñeiro[37,38], Gustavo Saiz[39], Haikuo Zhang[40], Hamada Abdelrahman[41], Haodi Xu[42], Inma Lebron[17], Irina Kurganova[43], Jennifer Blesh[44], Jeppe Å. Kristensen[45,46], Ji Liu[1], Jiacong Zhou[1], Jianping Wu[22], Jitendra Ahirwal[47], Junji Cao[48], Jørgen E. Olesen[49,50], Karin Kauer[51], Katerina Georgiou[52], Kees Jan van Groenigen[53], Kristof Van Oost[54], Kwame Agyei Frimpong[55], Lei Deng[56], Liane G. Benning[57], Liang Guo[56], Lizzie Mujuru[58], Manuel Delgado-Baquerizo[59], Maoz Dor[60], Mehdi Rahmati[61,62], Min Luo[63], Olga Kalinina[64], Olli Hyvärinen[65], Pablo García-Palacios[18,66], Paige Hansen[3], Patra Rounak[67], Pengpeng Duan[68], Pengzhi Zhao[54,69], Peter M. Homyak[11],

Rajan Ghimire[70], Renaldas Žydelis[71], Roland Bol[62], Ronaldo Vibart[9], Ruiying Chang[72], Ruyi Luo[73], Sebastián Villarino[74], Shuai Xue[75], Shuli Niu[76], Shuotong Chen[77], Tengfei Yu[78], Steven J. Hall[79], Thomas Kätterer[80], Tida Ge[81], Vusumuzi Erick Mbanjwa[82], Vyacheslav M. Semenov[43], Weixing Liu[83], Weiyu Shi[84], Wei Zhang[68], Wolfgang Wanek[85], Wolfram Buss[86], Xiangrong Cheng[87], Xiankai Lu[26], Xiaojun Shi[88], Xiaoli Cheng[22], Xiaorong Wei[56], Xiaotong Liu[89], Xuhui Zhou[90], Yahya Kooch[91], Yangquanwei Zhong[92], Yanjiang Cai[40], Yan Yang[76], Yiqi Luo[42], Yixuan Zhang[1], Yunbin Qin[93], Yunting Fang[94], Yuting Liang[95], Yuyi Li[83], Zengming Chen[95], Zhanfeng Liu[26], Zhaoliang Song[96], Zhongkui Luo[97], Zhisheng An[1] & Ji Chen[1,98,99]

[1]State Key Laboratory of Loess Science, Institute of Earth Environment, Chinese Academy of Sciences, Xi'an, China. [2]University of Chinese Academy of Sciences, Beijing, China. [3]Department of Soil and Crop Sciences, Colorado State University, Fort Collins, CO, USA. [4]Soil & Landscape Science, School of Molecular & Life Sciences, Faculty of Science & Engineering, Curtin University, Perth, WA, Australia. [5]Institute of Ecology, Chair of Soil Science, Technische Universität Berlin, Berlin, Germany. [6]Department of Geosciences and Natural Resource Management, University of Copenhagen, Copenhagen, Denmark. [7]Soil Science Laboratory, Graduate School of Agricultural Science, Kobe University, Kobe, Japan. [8]Department of Soil Science, University of Stellenbosch, Stellenbosch, South Africa. [9]AgResearch, Grasslands Research Centre, Palmerston North, New Zealand. [10]USDA Forest Service Rocky Mountain Research Station, Albuquerque, NM, USA. [11]Department of Environmental Sciences, University of California, Riverside, CA, USA. [12]Institute of Crop Science and Resource Conservation, Soil Science and Soil Ecology, University of Bonn, Bonn, Germany. [13]Department of Biology, College of Science, United Arab Emirates University, Al Ain, United Arab Emirates. [14]Laboratory of Soil Science, Ufa Institute of Biology, Ufa Federal Research Centre, Russian Academy of Sciences, Ufa, Russia. [15]Department of Geodesy, Cartography and Geographic Information Systems, Ufa University of Science and Technology, Ufa, Russia. [16]Institute of Grassland Science, Key Laboratory of Vegetation Ecology of the Ministry of Education, Jilin Songnen Grassland Ecosystem National Observation and Research Station, Northeast Normal University, Changchun, China. [17]UK Centre for Ecology and Hydrology, Environment Centre Wales, Bangor, Gwynedd, UK. [18]Instituto de Ciencias Agrarias (ICA), Consejo Superior de Investigaciones Científicas (CSIC), Madrid, Spain. [19]Department of Agricultural and Food Chemistry, Faculty of Sciences, Universidad Autónoma de Madrid, Madrid, Spain. [20]Department of Civil and Environmental Engineering, Massachusetts Institute of Technology, Cambridge, MA, USA. [21]Pollutant Inventories and Reporting Division, Environment and Climate Change Canada, Gatineau, QC, Canada. [22]Key Laboratory of Soil Ecology and Health in Universities of Yunnan Province, School of Ecology and Environmental Sciences, Yunnan University, Kunming, China. [23]Soil Science, TUM School of Life Sciences Weihenstephan, Technical University of Munich, Freising, Germany. [24]State Key Laboratory of Grassland Agro-Ecosystems, Engineering Research Center of Grassland Industry, Ministry of Education, College of Pastoral Agriculture Science and Technology, Lanzhou University, Lanzhou, China. [25]European Commission, Joint Research Centre (JRC), Ispra, Italy. [26]Key Laboratory of Vegetation Restoration and Management of Degraded Ecosystems, South China Botanical Garden, Chinese Academy of Sciences, Guangzhou, China. [27]College of Land and Environment, Shenyang Agricultural University, Shenyang, China. [28]College of Urban and Environmental Sciences, Northwest University, Xi'an, China. [29]Department of Ecology and Evolutionary Biology, Cornell University, Ithaca, NY, USA. [30]Environmental Sciences and Engineering, Biological and Environmental Science and Engineering Division, King Abdullah University of Science and Technology, Thuwal, Kingdom of Saudi Arabia. [31]Department of Global Development, College of Agriculture and Life Sciences, Cornell University, Ithaca, NY, USA. [32]Key Laboratory for Humid Subtropical Eco-Geographical Processes of the Ministry of Education, School of Geographical Sciences, Fujian Normal University, Fuzhou, China. [33]Facultad de Ciencias Agrarias, Universidad Nacional de Mar del Plata, Unidad Integrada Balcarce, Buenos Aires, Argentina. [34]College of Resources, Hunan Provincial Key Laboratory of Farmland Pollution Control and Agricultural Resources Use, Hunan Agricultural University, Changsha, China. [35]Key Laboratory of Coastal Environment Processes, Yantai Institute of Coastal Zone Research, Chinese Academy of Sciences, Yantai, China. [36]Department of Renewable Resources, University of Alberta, Edmonton, AB, Canada. [37]LART-IFEVA, Facultad de Agronomía, Universidad de Buenos Aires, CONICET, Buenos Aires, Argentina. [38]Departamento de Sistemas Ambientales, Facultad de Agronomía, Universidad de la República, Montevideo, Uruguay. [39]Departamento de Química Ambiental, Facultad de Ciencias, Universidad Católica de la Santísima Concepción, Centro de Energía, Concepción, Chile. [40]State Key Laboratory for Development and Utilization of Forest Food Resources, College of Carbon Neutrality, Zhejiang A&F University, Hangzhou, China. [41]Soil Science Department, Faculty of Agriculture, Cairo University, Giza, Egypt. [42]Soil and Crop sciences Section, School of Integrative Plant Science, Cornell University, Ithaca, NY, USA. [43]Institute of Physicochemical and Biological Problems in Soil Science of Russian Academy of Sciences, Pushchino, Russia. [44]School for Environment and Sustainability, University of Michigan, Ann Arbor, MI, USA. [45]Environmental Change Institute, School of Geography and the Environment, University of Oxford, Oxford, UK. [46]Center for Ecological Dynamics in a Novel Biosphere (ECONOVO), Section of Ecoinformatics and Biodiversity, Department of Biology, Aarhus University, Aarhus C, Denmark. [47]Centre of Environmental Studies, University of Allahabad, Prayagraj, India. [48]Institute of Atmospheric Physics, Chinese Academy of Sciences, Beijing, China. [49]Department of Agroecology, Aarhus University, Tjele, Denmark. [50]Global Change Research Institute of the Czech Academy of Sciences, Brno, Czech Republic. [51]Chair of Soil Science, Institute of Agricultural and Environmental Sciences, Estonian University of Life Sciences, Tartu, Estonia. [52]Physical and Life Sciences Directorate, Lawrence Livermore National Laboratory, Livermore, CA, USA. [53]Department of Geography, Faculty of Environment, Society and Economy, University of Exeter, Exeter, UK. [54]Earth and Life Institution, Université Catholique de Louvain, Louvain-la-Neuve, Belgium. [55]Department of Soil Science, School of Agriculture, University of Cape Coast, Cape Coast, Ghana. [56]State Key Laboratory for Soil Erosion and Dryland Farming on the Loess Plateau, Northwest A&F University, Yangling, China. [57]GFZ, Helmholtz Center for Geosciences, Potsdam, Germany. [58]Department of Environmental Science, Bindura University of Science Education, Bindura, Zimbabwe. [59]Laboratorio de Biodiversidad y Funcionamiento Ecosistémico, Instituto de Recursos Naturales y Agrobiología de Sevilla (IRNAS), Consejo Superior de Investigaciones Científicas (CSIC), Sevilla, Spain. [60]Department of Plant, Soil and Microbial Sciences, Michigan State University, East Lansing, MI, USA. [61]Department of Soil Science and Engineering, University of Maragheh, Maragheh, Iran. [62]Institute of Bio- and Geosciences, Agrosphere (IBG-3), Forschungszentrum Jülich, Jülich, Germany. [63]College of Environment and Safety Engineering, Fuzhou University, Fuzhou, China. [64]Department of Soil Science, CvO University of Oldenburg, Oldenburg, Germany. [65]Section for Aquatic Biology and Toxicology, Department of Biosciences, University of Oslo, Oslo, Norway. [66]Department of Plant and Microbial Biology, University of Zurich, Zurich, Switzerland. [67]Department of Biosystems Engineering and Soil Science, University of Tennessee, Knoxville, TN, USA. [68]Key Laboratory of Agro-ecological Processes in Subtropical Region, Institute of Subtropical Agriculture, Chinese Academy of Sciences, Changsha, China. [69]UK Centre for Ecology & Hydrology, Lancaster Environment Centre, Lancaster, UK. [70]Agricultural Science Center, New Mexico State University, Clovis, NM, USA. [71]Institute of Agriculture, Lithuanian Research Centre for Agriculture and Forestry, Akademija, Kedainiai District, Lithuania. [72]CAS Key Laboratory of Mountain Surface Processes and Ecological Regulation, Institute of Mountain Hazards and Environment, Chinese Academy of Sciences, Chengdu, China. [73]CAS Key Laboratory of Mountain Ecological Restoration and Bioresource Utilization & Ecological Restoration Biodiversity Conservation Key Laboratory of Sichuan Province, Chengdu Institute of Biology, Chinese Academy of

Sciences, Chengdu, China. [74]Consejo Nacional de Investigaciones Científicas y Técnicas (CONICET), BuenosAires, Argentina. [75]College of Bioscience & Biotechnology, Hunan Agricultural University, Changsha, China. [76]Key Laboratory of Ecosystem Network Observation and Modeling, Institute of Geographic Sciences and Natural Resources Research, Chinese Academy of Sciences, Beijing, China. [77]College of Environmental Science and Engineering, Yangzhou University, Yangzhou, China. [78]Key Laboratory of Ecological Safety and Sustainable Development in Arid Lands, Northwest Institute of Eco-Environment and Resources, Chinese Academy of Sciences, Lanzhou, China. [79]Department of Ecology, Evolution, and Organismal Biology, Iowa State University, Ames, IA, USA. [80]Department of Ecology, Swedish University of Agricultural Sciences, Uppsala, Sweden. [81]Key State Key Laboratory for Quality and Safety of Agro-Products, International Science and Technology Cooperation Base for the Regulation of Soil Biological Functions and One Health of Zhejiang Province, Ningbo University, Ningbo, China. [82]Soil Science Discipline, School of Agricultural, Earth and Environmental Sciences, University of KwaZulu-Natal, Pietermaritzburg, South Africa. [83]State Key Laboratory of Efficient Utilization of Arid and Semi-arid Arable Land in Northern China, the Institute of Agricultural Resources and Regional Planning, Chinese Academy of Agricultural Sciences, Beijing, China. [84]Chongqing Engineering Research Center for Remote Sensing Big Data Application and Chongqing Key Laboratory of Karst Environment, School of Geographical Sciences, Southwest University, Chongqing, China. [85]Division of Terrestrial Ecosystem Research, Department of Microbiology and Ecosystem Research, Center for Microbiology and Environmental Systems Science, University of Vienna, Vienna, Austria. [86]Research School of Biology, Australian National University, Canberra, ACT, Australia. [87]East China Coastal Forest Ecosystem Research Station, Institute of Subtropical Forestry, Chinese Academy of Forestry, Hangzhou, China. [88]College of Resources and Environment, Southwest University, Chongqing, China. [89]Institute of Resources and Environment, International Centre for Bamboo and Rattan, Key Laboratory of National Forestry and Grassland Administration/Beijing for Bamboo & Rattan Science and Technology, Beijing, China. [90]Northeast Asia Ecosystem Carbon Sink Research Center (NACC), Center for Ecological Research, Key Laboratory of Sustainable Forest Ecosystem Management-Ministry of Education, School of Forestry, Northeast Forestry University, Harbin, China. [91]Faculty of Natural Resources & Marine Sciences, Tarbiat Modares University, Mazandaran, Iran. [92]School of Ecology and Environment, Northwestern Polytechnical University, Xi'an, China. [93]Guangxi Key Laboratory of Landscape Resources Conservation and Sustainable Utilization in Lijiang River Basin, Guangxi Normal University, Guilin, Guangxi, China. [94]CAS Key Laboratory of Forest Ecology and Management, Institute of Applied Ecology, Chinese Academy of Sciences, Shenyang, China. [95]State Key Laboratory of Soil and Sustainable Agriculture, Institute of Soil Science, Chinese Academy of Sciences, Nanjing, China. [96]Institute of Surface-Earth System Science, School of Earth System Science, Tianjin University, Tianjin, China. [97]Institute of Agriculture Remote Sensing and Information Technology, College of Environmental and Resource Sciences, Zhejiang University, Hangzhou, China. [98]Guanzhong Plain Ecological Environment Change and Comprehensive Treatment National Observation and Research Station, Xi'an, China. [99]Institute of Global Environmental Change, Department of Earth and Environmental Science, School of Human Settlements and Civil Engineering, Xi'an Jiaotong University, Xi'an, China. ✉e-mail: chenji@ieecas.cn